Pérez Page, M.; Pérez Herranz, V. (2014). Study of the electrochemical behaviour of a 300 W PEM fuel cell stack by Electrochemical Impedance Spectroscopy. International Journal of Hydrogen Energy. 39(8):4009-4015. doi:10.1016/j.ijhydene.2013.05.121.

UNMARKED COPY

Study of the Electrochemical behavior of a 300 W PEM Fuel Cell Stack by Electrochemical Impedance Spectroscopy

M. Pérez-Page, V. Pérez-Herranz*

IEC Group. Departamento de Ingeniería Química y Nuclear. Universitat Politècnica de Valencia. Camino de Vera s/n. 46022 Valencia, Spain.

*Corresponding author. Tel.: +34-96-3877632; fax: +34-96-3877639;

e-mail address: vperez@iqn.upv.es (V. Pérez-Herranz)

Abstract.

Electrochemical impedance spectroscopy (EIS) is a suitable and powerful diagnostic testing method for fuel cells because it is non-destructive and provides useful information about fuel cell performance and its components. In this work, EIS measurements were carried out on a 300 W stack with 20 elementary cells. Electrochemical impedance spectra were recorded either on each cell or on the stack. Parameters of a Randles-like equivalent circuit were fitted to the experimental data. In order to improve the quality of the fit, the classical Randles cell was extended by changing the standard plane capacitor into a constant phase element (CPE). The effects of output current, cell position, operating temperature and humidification temperature on the impedance spectra were studied.

Key words: PEM fuel cells; Electrochemical Impedance Spectroscopy; Charge transfer resistance; Mass transfer resistance.

1. INTRODUCTION.

Among many kinds of fuel cells, the polymer electrolyte membrane fuel cell (PEMFC) has received much attention in the last two decades because of its lightweight, compactness, high power and low cost. PEMFCs have low emissions, high power density, a relatively simple design, quick start up, low noise emissions, and high-energy conversion efficiency (40%–60%) compared to traditional power sources. Therefore, PEMFCs are regarded as the most competitive candidates to replace the traditional forms of power conversion and they are being considered for near term service of several remote and mobile applications [1-5].

Polarization curves are the most common method for characterizing the electrochemical performance of fuel cells. However, there are some details of the fuel cell operation that cannot be detected by this technique. The major losses occurring in the electrochemical reactions of a fuel cell are due to the charge transfer through electrode–electrolyte interfaces, the transport of gases through the porous layer and the conduction of protons through the polymer electrolyte membrane. These losses and their dependency on the current density are described in terms of overvoltages. Nonetheless, a distinction of the single processes and their contribution to the overall losses is not possible by static measurements. To describe the dynamic electrochemical behavior of a fuel cell and to distinguish single loss factors, further information and dynamic measurements are needed [5-8].

Electrochemical Impedance Spectroscopy (EIS) or ac impedance is an electrochemical technique that can be used to characterize fuel cell performance non-invasively and in situ. In the case of fuel cells, in particular of the PEMFCs, it provides detailed information on the intrinsic loss factors, on the conductivity of the membrane, on the electrode processes, and on kinetic losses. The measurement of the impedance spectrum at an operating point and the identification of an appropriate impedance model enable the desired distinction of loss terms, and a description of the dynamic electrochemical behaviour of a fuel cell [9-16].

In this work, the electrochemical behavior of a single cell and a 300 W stack was studied measuring impedance spectra at different operating conditions. The frequency

response was modelled by an equivalent circuit and the model parameters were identified by nonlinear complex parameter identification as a function of the operation temperature, humidification temperature, current density and cell position.

2. EXPERIMENTAL.

Figure 1 shows a scheme of the experimental arrangement. It consisted of a 300 W fuel cell stack with 20 individual cells and an active area of 58 cm^2. The MEA consisted of a Nafion 115 membrane with a total Pt catalyst loading of 0.4 mg cm^{-2}. The stack was built from graphite composite bipolar plates with parallel flow channels. Cooling passages are provided by a central channel in each bipolar plate. Under optimal conditions with regard to pressure, humidity, reactants flow and temperature, the electrical output capability of the stack was 300 W. The supply of air to the cathode was handled by a compressor and the hydrogen was stored in a high-pressure tank at up to 200 bar. Using reduction valves, mass flow controllers, and an external humidifier, hydrogen and air were fed to the fuel cell stack. Purge valves were used to assist the removal of water droplets in the flow channels. The liquid cooling loop consisted of a continuous controlled pump and a heat exchanger. The temperatures were measured by thermocouples.

The system was fully instrumented to measure the process variables such as temperature and pressure of the different components, operating voltage and current of the PEMFC stack, and hydrogen and oxygen mass flows. A computer-based control and data acquisition system, based on a LabVIEW software developed application, collects and multiplexes the respective signals and feeds them into a PC responsible for the overall system control. A master control virtual instrument (VI) supervises the high-level control and data monitoring activities. The individual cell voltages were monitored through this system. Control of the individual components was achieved through the use of RS-232 communication ports.

Hydrogen was supplied to the fuel cell stack in the dead-end mode, while air was supplied with a stoichiometric ratio of 5. Before entering the stack, the reactant gases were passed through a humidifier where the humidification temperature was controlled.

Experiments were performed in galvanostatic mode using an Agilent N3300A electronic load. Impedance measurements were carried out using an Autolab PGSTAT302 potentiostat with an Autolab FRA2 (frequency response analyser) module combined with the electronic load. The frequency range from 5 kHz to 0.25 Hz was

covered by 50 points. The current was modulated through the stack and the voltage was measured either across a single cell (EIS of cell) either across the stack (EIS of the stack). The AC signal amplitude was optimized for this study at high current. To achieve a steady-state before starting each impedance measurement, the fuel cell stack was operated at 0.25 A cm^2 (individual cell potential about 0.6 V) for about 30 min., until a steady-state voltage was obtained. After this stabilization period, the stack was operated at the working point for 5 min to ensure that the voltage was stable. After this, an EIS spectrum was measured. This measurement cycle was repeated three times in order to check and ensure a good reproducibility of the measurements. The voltages before and after the EIS measurement were determined to verify the stability of the cell. Experiments were carried out at three current densities of 0.0862, 0.1724 and 0.2586 A/cm^2, different operation temperatures from 40 to 70ºC and two humidification temperatures of 50ºC and 60ºC. The operation pressure was 1 bar.

3. RESULTS AND DISCUSSION.

Electrochemical impedance spectroscopy was applied to separate and to quantify the processes governing the fuel cell response. The study was conducted at three current densities of 0.0862, 0.1724 and 0.2586 A/cm^2. Typical impedance spectra measured in the fuel cell stack and in a single cell are presented in Figures 2a and b, where two depressed semicircles can be observed. The impedance spectra of PEMFCs are practically entirely determined by the cathode losses, which are the main contribution to overpotential. The high frequencies loop or kinetic loop corresponds to the charge transfer process of the oxygen reduction reaction. The low frequencies loop is related with the mass transport and gas diffusion processes. The low frequencies loop appears to be most interesting, since it may provide information on diffusional processes responsible for an important part of the total resistance. However, the origin of this loop is controversial; the loop was assigned to the slow diffusion of oxygen through the backing, back diffusion of water through the membrane, or diffusion of water in the catalyst layer [17-19]. As can be seen in Figure 2a, the impedance of the fuel cell stack is about 20 times the impedance of a single cell. In this case, the stack involves 20 elementary cells assumed to be equivalent and consequently its impedance is 20 times the impedance of a single cell.

The impedance spectra presented in Figures 2a and b suggest two time constants and can be modelled by the equivalent circuit shown in Figure 2c [20-23]. The depressed semicircles can been explained by a number of phenomena, depending on the nature of the system being investigated, as for instance in-homogeneous electrode surface or distribution of activation or relaxation processes. However, the common thread among these explanations is that some property of the system is not homogeneous or that there is a distribution of the value of some physical parameter. These depressed semicircles are usually dealt with by changing the standard plane capacitor of the Randles cell with Warburg finite-length diffusion element into a constant phase element (CPE) [24, 25], as seen in Figure 2c. Therefore, the electric circuit is composed by the membrane or ohmic resistance, R_m, that represents the total ohmic resistance of the fuel cell and it is the high frequency intercept of the kinetic loop with the real axis; R_{ct} is the charge transfer resistance due to the oxygen reduction reaction; CPE1 is a constant phase element which reflects the R_{ct} associated to the

catalyst layer capacitance properties and W_s is the Warburg impedance, that is related to mass transfer and diffusion processes [26-28].

The impedance of a constant phase element is given by equation 1, where CPE_T y φ are constant phase element parameters [9, 14, 27].

$$Z_{CPE} = \frac{1}{\left[CPE_T \cdot (j \cdot \omega)^{\varphi}\right]} \tag{1}$$

The Warburg impedance is the impedance arising from one-dimensional diffusion of a species to the electrode. The general case, describing the effect of the diffusion of species is shown in equation 2, where R_{tm} is the mass transport resistance and T_w is a Warburg parameter that is described in equation 3 where δ is a diffusion lengthy and D_a is de diffusivity.

$$Z_W = R_{tm} \cdot \left[\frac{\tanh(T_W \cdot j \cdot \omega)^{0.5}}{(j \cdot \omega \cdot T_W)^{0.5}} \right] \tag{2}$$

$$T_W = \frac{\delta^2}{D_a} \tag{3}$$

The impedance spectra of a single cell and their fitting curves at three different current densities, when fuel cell is working at operation and humidification temperatures of 60ºC, are presented in Figure 3. The impedance spectra have been corrected with respect to the ohmic resistance. It can be seen that an increment of current density reduces the diameter of the kinetic loop which reveals the decrement of the charge transfer resistance. As current density increases, the driving force of the oxygen reduction reaction gradually increases, therefore, the charge transfer resistance of the cell decreases. On the other hand, an increment of current density increases the low frequency loop related with the mass transport and gas diffusion processes.

For the lowest current density of 0.0862 A/cm^2, the diameter of the kinetic loop is higher than the diameter of the mass transfer loop. Conversely, for the highest current density of 0.2586 A/cm^2, the diameter of the kinetic loop is lower than the diameter of the mass transfer loop. As current density increases, the driving forces of the oxygen reduction reaction gradually increase, so the charge transfer of the fuel cell gradually decreases. Also, the amount of generated water will increase; therefore, mass transport

limitation will become more significant, which causes the mass transport resistance increases gradually with the increase of current density [11, 12, 28].

The experimental impedance data were fitted to the equivalent circuit of Figure 2c using the complex nonlinear least square (CNLS) fitting method with Zview software package, and the different parameters of the equivalent circuit were obtained. Figures 4a-c show the effect of current density on the ohmic resistance (a), charge transfer resistance (b) and mass transfer resistance (c) at different operation temperatures and a humidification temperature of 60ºC. In these figures can be seen that the ohmic resistance and the charge transfer resistance decrease as the current density increases. However, the mass transfer resistance increases with current density.

The generated water increases as the current density increase which improves the hydration level of the membrane. Also, the membrane conductivity improves with the water content and this improvement may be the result of an increase of the proton mobility, leading to the decrease of the ohmic resistance with the increase of current density and with the decrease of the operation temperature, as can be seen in Figure 4a [12, 14]. This would also explain why the effect of the operation temperature on the ohmic resistance is greater at the lowest current density. In Figure 4b can be seen that the charge transfer decreases with the increase of current density and with the decrease of the operation temperature because the increase of the current density improves the kinetic of the oxygen reduction reaction that it is produced on the cathode [29, 30]. The effect of the operation temperature on the charge transfer resistance is greater at the lowest current density. On the other hand, the operation temperature has little effect on the mass transport resistance, especially at low current densities, as can be seen in Figure 4c, but the mass transport resistance increases with current density due to limitation of oxygen transport to the catalyst layer. The current density increase produces an increase in the water content that favours the membrane hydration; however, at higher current densities, water can be accumulated on the cathode. This water accumulation can block the catalytic active sites, then, the oxygen reduction reaction may not be produced. This effect produces that the mass transfer resistance increases [31-33].

EIS has been used to study the effect of the cell position on the performance of the fuel cell stack. This study was carried out by measuring the impedance spectra in three different cells of the fuel cell stack, cell 1, located at the cooling water inlet, cell 20, located at the cooling water outlet, and cell 10, located in the center of the stack. Figures 9a-b show the impedance spectra and their fitting curves of the three cells obtained at the current densities of 0.0862 A/cm^2 and 0.2586 A/cm^2 respectively. The impedance spectra have been corrected with respect to the ohmic resistance. As can be seen in Figure 5a, for low current densities, the three cells have a similar performance. However, as can be seen in Figure 5b, at the highest current density of 0.2586 A/cm^2, cell 1 provides the highest impedance, and therefore, the worst performance. At this current density, cell 10 has the lowest impedance and therefore better performance.

The differences found in the three cells at the different current densities can be explained from the temperature variation along the stack. The inlet temperature, which coincides approximately with the temperature of the cell 1, remains almost constant with current density. However, the outlet temperature, which coincides with the temperature of the cell 20, increases with current density. At low current densities, the temperature difference between the inlet and outlet of the water cooling loop is minimal and remains almost constant with current density. Therefore, at low current densities, all cells operate at similar temperatures; the cells show a similar behaviour and the impedance spectra of all cells are similar as shown in Figure 5a. However, at high current densities, cell 1 operates at the lowest temperature and the cell 20 at the highest temperature. This would explain the differences observed in the impedance spectra of the three cells shown in Figure 5b. For the conditions shown in Figure 5b, cell 10 show the best performance because the best combination of humidification and operation temperatures.

Figures 6a-b show the effect of the cell position on the ohmic resistance, charge transfer resistance and mass transport resistance for two current densities of 0.0862 A/cm^2 and 0.2586 A/cm^2 respectively, for a humidification temperature of 50ºC and an operation temperature of 40ºC. As shown in Figure 6a, for the lowest current density of 0.0862 A/cm^2, the ohmic resistance is much greater than the charge transfer and mass transport resistances, for the reasons discussed previously. However, for the highest current density of 0.2586 A/cm^2, is the mass transport resistance which presents higher

values, as shown in Figure 6b. Furthermore, for the highest current density of 0.2586 A/cm^2, cell 10 presents the lowest values of the ohmic, charge transfer and mass transport resistances due to variations in temperature within the stack which have been mentioned previously.

4. CONCLUSIONS.

Electrochemical Impedance Spectroscopy has been used to study of the electrochemical behaviour of a PEMFC stack. The impedance spectra of the fuel fell stack and single cells have been obtained. These spectra present two loops, the first loop at high frequencies, which is related with the oxygen reduction reaction kinetics, and the second loop at low frequencies, which is related with mass transport and diffusion processes.

The experimental impedance data have been fitted at an equivalent circuit in which the standard plane capacitor of the Randles cell with Warburg finite-length diffusion element into a constant phase element (CPE). The experimental impedance data were fitted to the equivalent circuit, and the different parameters of the equivalent circuit were obtained.

Current density affects the impedance spectra. An increment of current density reduces the diameter of the kinetic loop obtained at high frequencies, which reveals the decrement of the charge transfer resistance. On the other hand, an increment of current density increases the high frequency loop related with the mass transport and gas diffusion processes. Ohmic and charge transfer resistances decrease with current density due to improved membrane humidification and oxygen reduction reaction kinetics. Mass transport resistance increases with current density due to mass transport limitations caused by water accumulation.

Changes in temperature along the fuel cell stack with current density causes the cells that compose the stack behave differently, especially at high current densities. As a result, the ohmic, charge transfer and mass transport resistances change with the position of the cells.

5. REFERENCES.

[1] M. J. Khan and M. T. Iqbal, Dynamic modeling and simulation of a small wind-fuel cell hybrid energy system, *Renewable Energy*, 30 (2005) 421-439.

[2] J. K. Soeng and O. B. Soo, Fuel economy and life-cycle cost analysis of a fuel cell hybrid vehicle, *Journal of Power Sources*, 105 (2002) 58-65.

[3] P. Ekdunge and M. Raberg, The fuel cell vehicle analysis of energy use, emissions and cost, *International Journal of Hydrogen Energy*, 23 (1998) 381-385.

[4] M. A. R. S. Al Baghdadi and H. A. K. S. Al Janabi, Parametric and optimization study of a PEM fuel cell performance using three-dimensional computational fluid dynamics model, *Renewable Energy*, 32 (2007) 1077-1101.

[5] Q. G. Yan, H. Toghiani and H. Causey, Steady state and dynamic performance of proton exchange membrane fuel cells (PEMFCs) under various operating conditions and load changes, *Journal of Power Sources*, 161 (2006) 492-502.

[6] L. Wang, A. Husar, T. H. Zhou and H. T. Liu, A parametric study of PEM fuel cell performances, *International Journal of Hydrogen Energy*, 28 (2003) 1263-1272.

[7] J. Zhang, Y. Tang, C. Song, X. Cheng, J. Zhang and H. Wang, PEM fuel cells operated at 0% relative humidity in the temperature range of 23-120 ºC, *Electrochimica Acta*, 52 (2007) 5095-5101.

[8] M. Amirinejad, S. Rowshanzamir and M. H. Eikani, Effects of operating parameters on performance of a proton exchange membrane fuel cell, *Journal of Power Sources*, 161 (2006) 872-875.

[9] J. Wu, X. Z. Yuan, H. Wang, M. Blanco, J. J. Martin and J. Zhang, Diagnostic tools in PEM fuel cell research: Part I Electrochemical techniques, *International Journal of Hydrogen Energy*, 33 (2008) 1735-1746.

[10] M. A. Danzer and E. P. Hofer, Analysis of the electrochemical behaviour of polymer electrolyte fuel cells using simple impedance models, *Journal of Power Sources*, 190 (2009) 25-33.

[11] X. Yuan, H. Wang, J. C. Sun and J.n Zhang, AC impedance technique in PEM fuel cell diagnosis.A review, *International Journal of Hydrogen Energy*, 32 (2007) 4365-4380.

[12] M. Ciureanu and R. Roberge, Electrochemical impedance study of PEM fuel cells. Experimental diagnostics and modeling of air cathodes, *Journal of Physical Chemistry B*, 105 (2001) 3531-3539.

[13] X. Yan, M. Hou, L. Sun, D. Liang, Q. Shen, H. Xu, P. Ming and B. Yi, AC impedance characteristics of a 2 kW PEM fuel cell stack under different operating

conditions and load changes, *International Journal of Hydrogen Energy*, 32 (2007) 4358-4364.

[14] S. Asghari, A. Mokmeli and M. Samavati, Study of PEM fuel cell performance by electrochemical impedance spectroscopy, *International Journal of Hydrogen Energy*, 35 (2010) 9283-9290.

[15] A. Hakenjos, M. Zobel, J. Clausnitzer and C. Hebling, Simultaneous electrochemical impedance spectroscopy of single cells in a PEM fuel cell stack, *Journal of Power Sources*, 154 (2006) 360–363.

[16] S. J. Andreasen, J. L. Jespersen, E. Schaltz, and S. K. Kær, Characterisation and Modelling of a High Temperature PEMFuel Cell Stack using Electrochemical Impedance Spectroscopy, *Fuel Cells*, 9 (2009) 463–473.

[17] N. Wagner, W. Schnurnberger, B. Muller and M. Lang, Electrochemical impedance spectra of solid-oxide fuel cells and polymer membrane fuel cells, *Electrochimica Acta*, 43 (1998) 3785-3793.

[18] T. E. Springer, T. A. Zawodzinski, M. S. Wilson and S. Gottesfeld, Characterization of polymer electrolyte fuel cells using AC impedance spectroscopy, *Journal of the Electrochemical Society*, 143 (1996) 587-599.

[19] V. A. Paganin, C. L. F. Oliveira, E. A. Ticianelli, T. E. Springer and E. R. Gonzalez, Modelisticinterpretation of the impedance response of a polymer electrolyte fuel cell, *Electrochimica Acta*, 43 (1998) 3761-3766.

[20] A Lasia, Electrochemical Impedance Spectroscopy and its Application. En: B.E.Conway et al (ed), *Moderm Apects of Electrochemistry.*, New York, 1999.

[21] M Sluyters-Rehbach, Impedances of Electrochemical Systems: Terminology, Nomengrature and Representation. Part I: Cells with metal electrodes and liquid solutions, *Pure and Applied Chemistry*, 66 (1994) 1831-1891.

[22] D. R. Franceschetti and J. R. Macdonald, Electrode kinetics, equivalent circuits, and system characterization: Small-signal conditions, *Journal of Electroanalytical Chemistry and Interfacial Electrochemistry*, 82 (1977) 271-301.

[23] D. Vladikova, The technique of the differential impedance analysis. Part I: Basics of the impedance spectroscopy, *Proceedings of the International Workshop "Advanced Techniques for Energy Sources Investigation and Testing" 4-9 Sept.2004, Sofia, Bulgaria* (204).

[24] J. R. Macdonald, *Impedance Spectroscopy Theory, Experiment and Applications*, John Wiley and Sons, Inc., Hoboken, New Yersey, 2005.

[25] N. Wagner, Characterization of membrane electrode assemblies in polymer electrolyte fuel cells using a.c. impedance spectroscopy, *Journal of Applied Electrochemistry*, 32 (2002) 859-863.

[26] N. Fouquet, C. Doulet, C. Nouillant, G. Dauphin-Tanguy and B. Ould-Bouamama, Model based PEM fuel cell state-of-health monitoring via ac impedance measurements, *Journal of Power Sources*, 159 (2006) 905-913.

[27] S. D. Mikhailenko, M. D. Guiver and S. Kaliaguine, Measurements of PEM conductivity by impedance spectroscopy, *Solid State Ionics*, 179 (2008) 619-624.

[28] M. A. Rubio, A. Urquia and S. Dormido, Diagnosis of performance degradation phenomena in PEM fuel cells, *International Journal of Hydrogen Energy*, 35 (2010) 2586-2590.

[29] X. Yuan, J. C. Sun, M.o Blanco, H. Wang, J. Zhang and D. P. Wilkinson, AC impedance diagnosis of a 500 W PEM fuel cell stack: Part I: Stack impedance, *Journal of Power Sources*, 161 (2006) 920-928.

[30] X. Yuan, J. C. Sun, H. Wang and J. Zhang, AC impedance diagnosis of a 500 W PEM fuel cell stack: Part II: Individual cell impedance, *Journal of Power Sources*, 161 (2006) 929-937.

[31] T. J. P. Freire and E. R. Gonzalez, Effect of membrane characteristics and humidification conditions on the impedance response of polymer electrolyte fuel cells, *Journal of Electroanalytical Chemistry*, 503 (2001) 57-68.

[32] D. R. Sena, E. A. Ticianelli, V. A. Paganin and E. R. Gonzalez, Effect of water transport in a PEFC at low temperatures operating with dry hydrogen, *Journal of Electroanalytical Chemistry*, 477 (1999) 164-170.

[33] H. Xu, H. R. Kunz and J. M. Fenton, Analysis of proton exchange membrane fuel cell polarization losses at elevated temperature 120 ºC and reduced relative humidity, *Electrochimica Acta*, 52 (2007) 3525-3533.

Acknowledgements.

This work was supported by Generalitat Valenciana (PROMETEO/2010/023).

List of Figures.

UNMARKED COPY

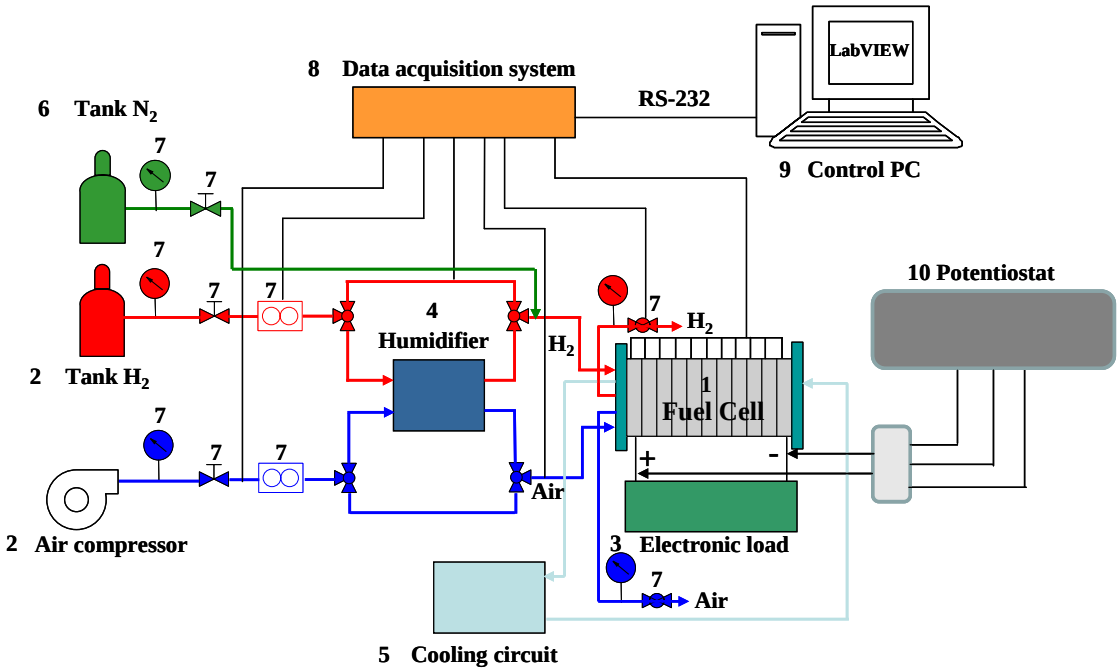

Figure 1. Scheme of the experimental arrangement.

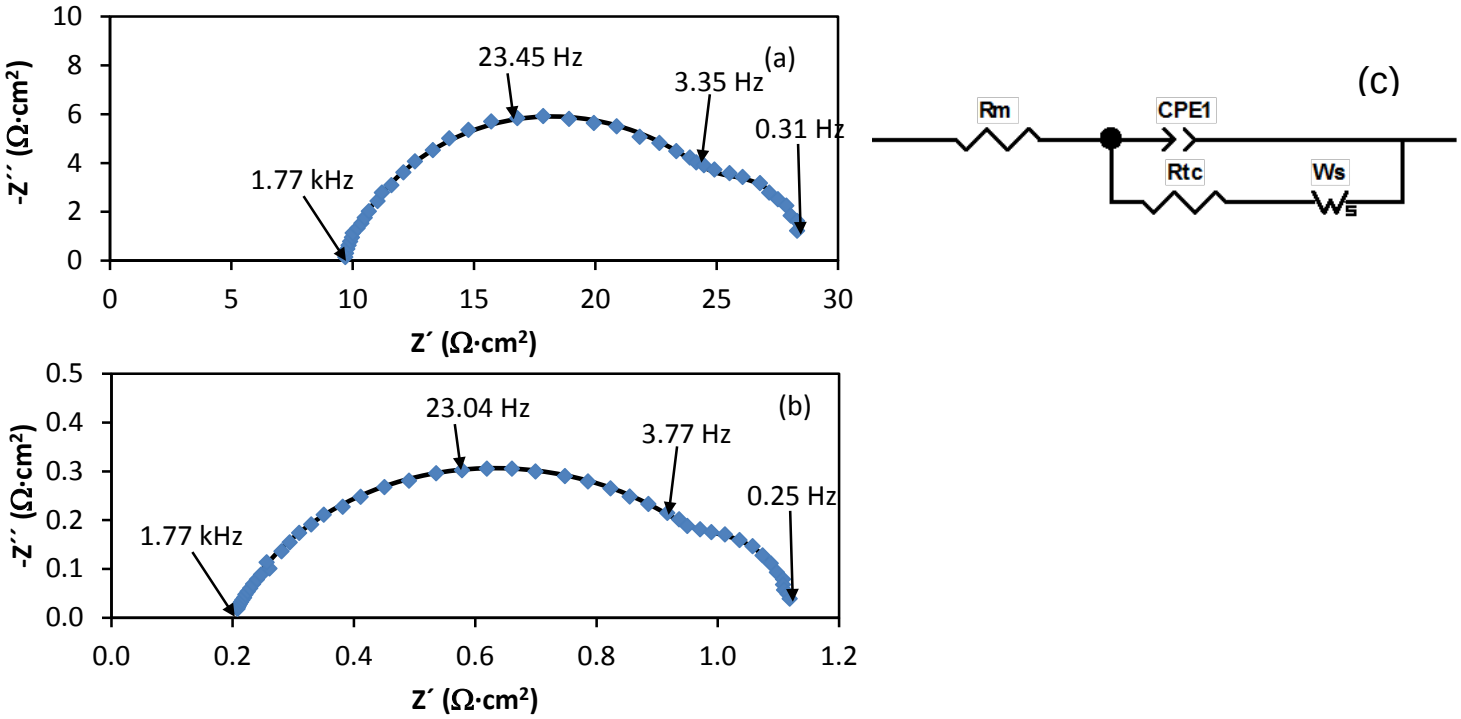

Figure 2. Impedance spectra and equivalent circuit. Impedance spectra of the fuel cell stack (a). Impedance spectra of a single cell (b). Equivalent circuit (c).

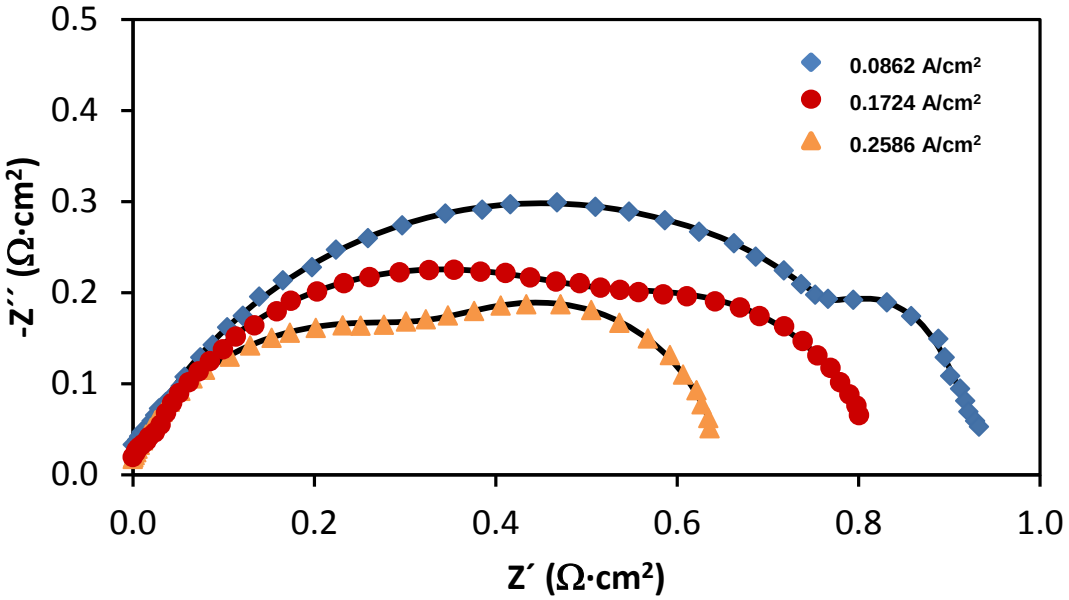

Figure 3. Effect of current density on the impedance spectra of a single cell.

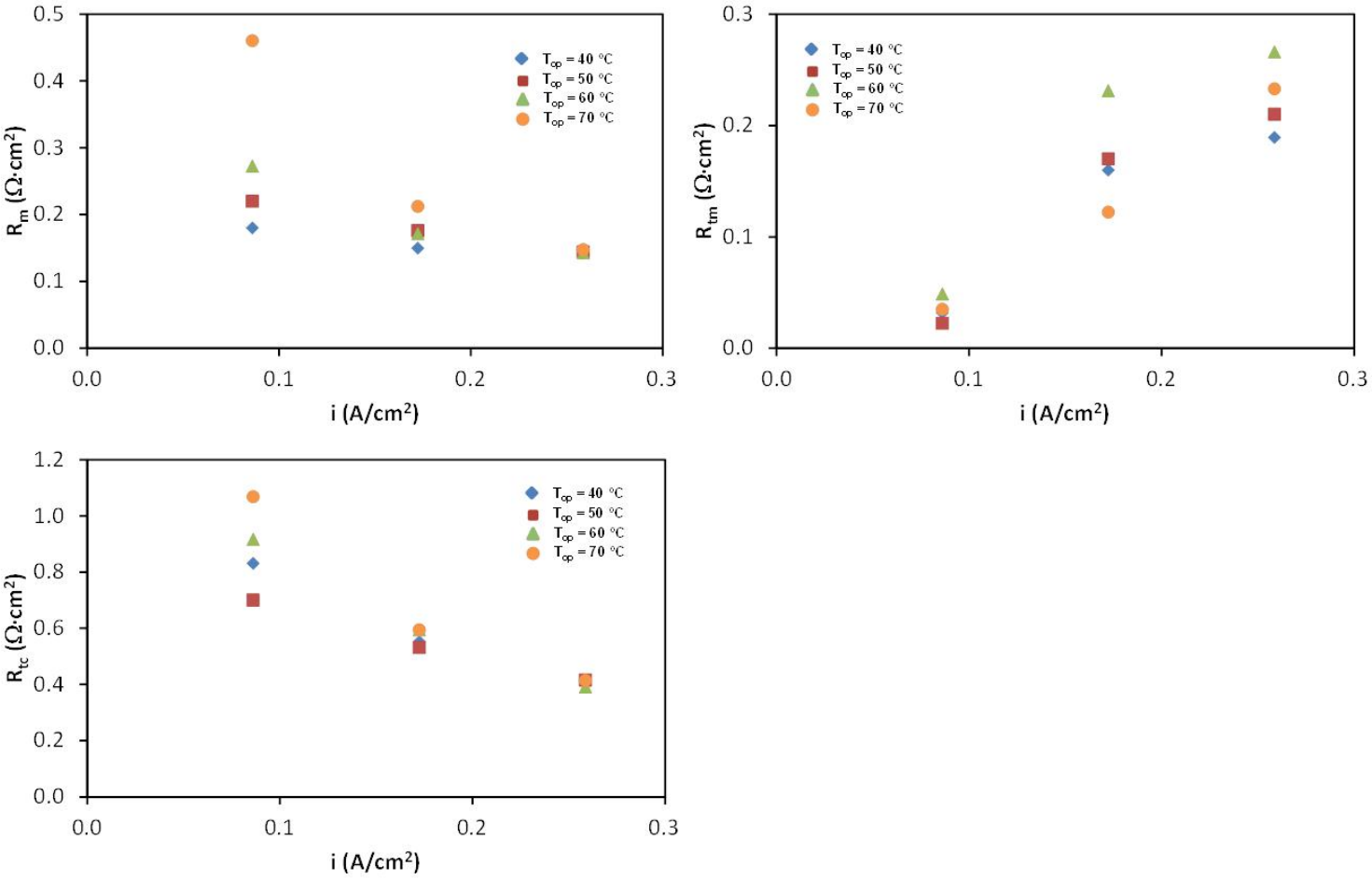

Figure 4. Effect of current density on the ohmic resistance (a), charge transfer resistance (b), and mass transport resistance (c) at a humidification temperature of 60ºC and different operation temperatures.

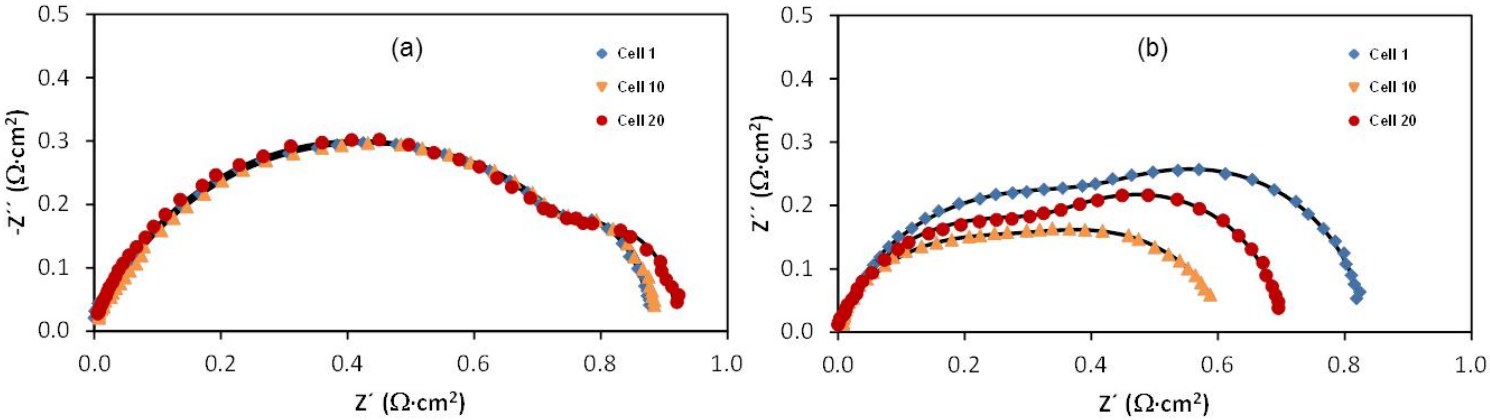

Figure 5. Effect of the cell position on the impedance spectra for current densities of 0.0862 A/cm^2 (a) and 0.2586 A/cm^2 (b) at a humidification temperature of 50ºC and an operation temperature of 40ºC.

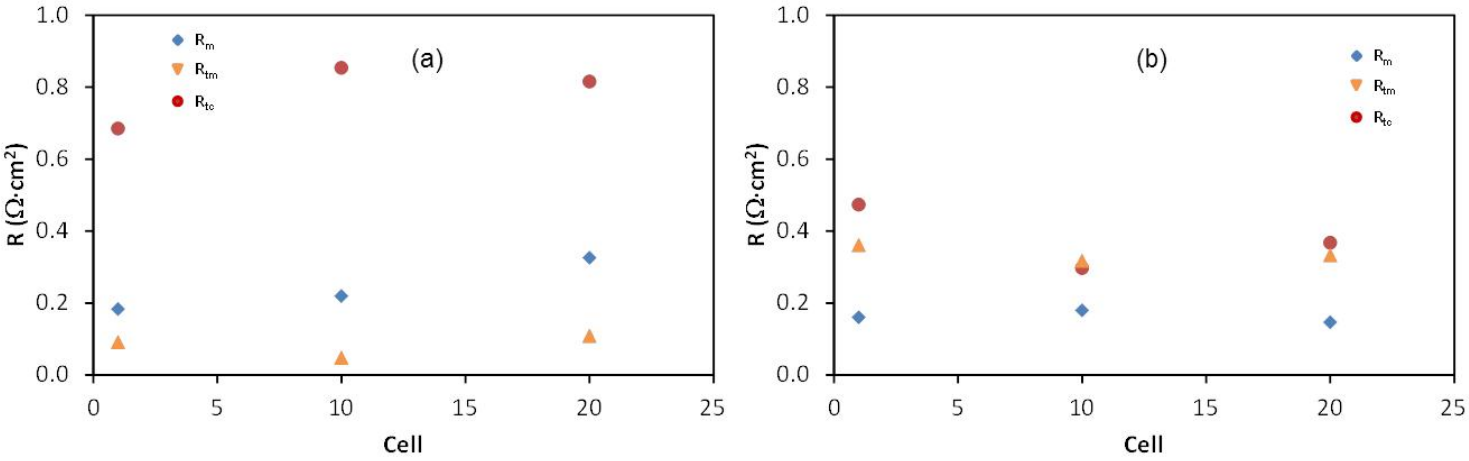

Figure 6. Effect of the cell position on the ohmic resistance, charge transfer resistance and mass transport resistance for current densities of 0.0862 A/cm^2 (a) and 0.2586 A/cm^2 (b) at a humidification temperature of 50ºC and an operation temperature of 40ºC.